



# Anti-PbO-type CoSe film: a possible analog to FeSe superconductors

Chong Liu<sup>1</sup> , Fawei Zheng<sup>2</sup>, Lei Shen<sup>1</sup>, Menghan Liao<sup>1</sup>, Rui Wu<sup>1</sup>,  
Guanming Gong<sup>1</sup>, Cui Ding<sup>1</sup>, Haohao Yang<sup>1</sup>, Wei Li<sup>1,3</sup> , Can-Li Song<sup>1,3</sup>,  
Ke He<sup>1,3</sup>, Xu-Cun Ma<sup>1,3</sup>, Ding Zhang<sup>1,3</sup>, Lexian Yang<sup>1,3</sup>, Ping Zhang<sup>2</sup>,  
Lili Wang<sup>1,3,4</sup>  and Qi-Kun Xue<sup>1,3,4</sup>

<sup>1</sup> State Key Laboratory of Low-Dimensional Quantum Physics, Department of Physics, Tsinghua University, Beijing 100084, People's Republic of China

<sup>2</sup> Institute of Applied Physics and Computational Mathematics, Beijing 100088, People's Republic of China

<sup>3</sup> Collaborative Innovation Center of Quantum Matter, Beijing 100084, People's Republic of China

E-mail: [liliwang@mail.tsinghua.edu.cn](mailto:liliwang@mail.tsinghua.edu.cn) and [qkxue@mail.tsinghua.edu.cn](mailto:qkxue@mail.tsinghua.edu.cn)

Received 2 August 2018, revised 26 August 2018

Accepted for publication 13 September 2018

Published 15 October 2018



## Abstract

Quasi-two-dimensionality is well known as a key electronic and structural element of high temperature superconductivity. Here we prepared ultrathin films of anti-PbO-type CoSe down to the monolayer on a SrTiO<sub>3</sub>(001) substrate using molecular beam epitaxy, and investigated their electronic structures by scanning tunneling microscopy, angle-resolved photoemission spectroscopy, and transport measurements in combination with first-principles calculations. We found that the monolayer CoSe had similar band structure and non-ferromagnetism nature with monolayer FeSe on SrTiO<sub>3</sub>, except for the Fermi level upshift by  $\sim 0.25$  eV and weaker electronic correlation with a renormalization factor of 1.7, due to extra electron filling from Co 3d<sup>7</sup> compared with Fe 3d<sup>6</sup>. The results hint that superconductivity might emerge in hole-doped tetragonal CoSe films.

Supplementary material for this article is available [online](#)

Keywords: tetragonal CoSe, molecular beam epitaxy (MBE), scanning tunneling microscopy (STM), band structure

(Some figures may appear in colour only in the online journal)

## 1. Introduction

Cuprates and iron-based superconductors, the two families of unconventional high temperature (high  $T_c$ ) superconductors discovered so far, share layered structures made up of two types of quasi-two-dimensional (2D) substructures, superconducting layers (CuO<sub>2</sub> layer or FeAs/FeSe layer) and charge reservoir layers [1, 2], where the former host high temperature superconductivity with charge carriers transferred from the latter [3, 4]. The quasi-two-dimensionality thus is, on empirical grounds, known as a key structural and electronic element that supports high  $T_c$  superconductivity. Under such a scenario, interface engineering and interlayer intercalations are widely applied, and indeed lead

to the discovery of various 2D systems with enhanced or newly emerged superconductivity. Taking FeSe, a superconductor with  $T_c$  of 8 K [5], as an example, the  $T_c$  remarkably rises to 20–50 K under alkali metal intercalation between FeSe layers and formation of AFe<sub>2</sub>Se<sub>2</sub> (A = alkali metal) with the ThCr<sub>2</sub>Si<sub>2</sub>-type structure [6, 7], and even above 65 K when interfaced with SrTiO<sub>3</sub> [8]. With extensive research on various interface enhanced superconductors, like LaAlO<sub>3</sub>/SrTiO<sub>3</sub> [9], La<sub>1.9</sub>Sr<sub>0.1</sub>CuO<sub>4</sub>/SrLaAlO<sub>4</sub> [10], La<sub>2</sub>CuO<sub>4</sub>/La<sub>1.55</sub>Sr<sub>0.45</sub>CuO<sub>4</sub> [11] and FeSe/SrTiO<sub>3</sub> [12, 13], it is widely accepted that interface charge transfer plays the essential role [8, 14], as it does in high  $T_c$  cuprates and iron-based superconductors with the built-in multi-interfaces. Additionally, the electron pairing may be mediated by extrinsic phonon modes [15] and magnetic fluctuations [16] that are injected through interface or intrinsic ones

<sup>4</sup> Authors to whom any correspondence should be addressed.

that are modulated due to interlayer coupling and substrate template effect [17], which could promote  $T_c$  as well.

CuO<sub>2</sub> and FeSe/FeAs layers, the basic building blocks of high  $T_c$  cuprates and iron-based superconductors, share similarities as well. They are late transition metal compounds with square sub-lattices of d-cations under 3d<sup>9</sup> (Cu<sup>2+</sup>) and 3d<sup>6</sup> (Fe<sup>2+</sup>) configurations, and the  $d_{x^2-y^2}$  and  $d_{xy}/d_{xz}/d_{yz}$  orbitals hold the key ingredients of high temperature superconductivity, respectively [18, 19]. In addition to 3d<sup>9</sup> (Cu<sup>2+</sup>) and 3d<sup>6</sup> (Fe<sup>2+</sup>) electron systems, 3d<sup>8</sup> (Ni<sup>2+</sup>) electrons can host superconductivity. ANi<sub>2</sub>As<sub>2</sub> and ANi<sub>2</sub>Se<sub>2</sub>, the alkali metal intercalated Ni pnictides and chalcogenides [20, 21], both in the ThCr<sub>2</sub>Si<sub>2</sub>-type structure, host heavy electron superconductivity with  $T_c < 4$  K, bridging between Fe-based and standard heavy-fermion superconductors. These results motivate one to question whether the analog compounds of cobalt, which is located between Fe and Ni in the periodic table, can have superconducting transitions. Nonetheless, few reports on superconducting Co compounds are available. Up to now, only Na<sub>x</sub>(H<sub>3</sub>O)<sub>2</sub>CoO<sub>2</sub>·yH<sub>2</sub>O (2D CoO<sub>2</sub> layer as basic building block) [22] and LaCo<sub>2</sub>B<sub>2</sub> with cationic substitution (2D CoB layer as basic building block) [23] are superconducting with  $T_c < 5$  K. ACo<sub>2</sub>Se<sub>2</sub>, the cobalt analogs of A<sub>x</sub>Fe<sub>2-y</sub>Se<sub>2</sub> and ANi<sub>2</sub>Se<sub>2</sub> that have the same quasi-2D ThCr<sub>2</sub>Si<sub>2</sub>-type crystal structure, are itinerant ferromagnetic metals [24] but not superconductors. Bulk CoSe, which has NiAs-type hexagonal structure [25] instead of the layered anti-PbO-type tetragonal structure, does not superconduct at all. Compared with an FeSe superconductor, ACo<sub>2</sub>Se<sub>2</sub> must be in the electron over-doped regime, since both Co 3d<sup>7</sup> substitution of Fe 3d<sup>6</sup> and alkali metal intercalation lead to electron doping. With the phase diagram of superconductivity with doping level concerned [2], the most important preliminary step to explore possible CoSe based superconductor is obtaining CoSe consisted of stacked quasi-2D layers, i.e. replacing the NiAs-type hexagonal structure with an anti-PbO-type tetragonal one.

In this work, we successfully fabricated anti-PbO-type CoSe thin films with thicknesses ranging from single unit cell (UC) to 5 UC on SrTiO<sub>3</sub>(001) using molecular beam epitaxy (MBE). We investigated the electronic properties through scanning tunneling microscopy/spectroscopy (STM/STS), angle-resolved photoemission spectroscopy (ARPES) and transport measurements in combination with first-principles calculations. We found that the tetragonal phase films were non-ferromagnetic metal. In particular, the monolayer CoSe films had similar band structures to monolayer FeSe on SrTiO<sub>3</sub>, except that the Fermi level shifted upward and the electronic correlation weakened, for Co atom has one more electron in the 3d shell than Fe atom. Our results suggest that anti-PbO-type CoSe could probably host superconductivity under hole doping.

## 2. Experiments and calculations

The Nb:SrTiO<sub>3</sub>(001) single crystals were chosen as substrates (Nb 0.5 wt% for STM and ARPES measurements, and

0.05 wt% for transport measurements). After being annealed at 1100 °C to obtain a TiO<sub>2</sub>-terminated surface, the substrates were kept at 360 °C during film growth. The CoSe films were grown by co-evaporating Co (99.995%) and Se (99.999%) from Knudsen cells at respective cell temperatures of 1120 °C and 100 °C. The Co:Se flux ratio was ~1:5 and the growth rate was 0.12 UC min<sup>-1</sup>. After the MBE growth, the samples were *in situ* transferred into the STM head for data collection at 4.8 K. A PtIr tip was used throughout the experiments. STM topographic images were acquired in a constant current mode, with the bias voltage ( $V_s$ ) applied to the sample. Tunneling spectra were measured by disabling the feedback circuit, sweeping the sample voltage  $V_s$ , and extracting the differential conductance  $dI/dV$  using a standard lock-in technique with a small bias modulation (~1% of the sweeping range) at 937 Hz.

The samples were transferred through a vacuum suitcase (the base pressure was lower than 10<sup>-8</sup> mbar) for ARPES measurements with photons of 21.2 eV from a helium-discharging lamp. The data were recorded by a Scienta DA30 analyzer. The total convolved energy and angle resolutions were 15 meV and 0.2°, respectively. For *ex situ* transport measurement, ~10 nm thick amorphous Se was deposited on the CoSe films at 100 K as a protection layer, and freshly cut indium cubes were pressed onto the sample as contacts. A standard six-terminal lock-in method was employed with a typical current of 1 μA at 13 Hz. The current went through the CoSe thin films due to the non-ohmic contact with the SrTiO<sub>3</sub> substrate (see the supplementary material available online at [stacks.iop.org/SUST/31/115011/mmedia](https://stacks.iop.org/SUST/31/115011/mmedia)), which guaranteed the transport characterization of CoSe films rather than SrTiO<sub>3</sub>.

The density functional theory (DFT) calculations were performed by using the projected augmented wave method [26–28] as implemented in VASP code [29]. We adopted the Perdew–Burke–Ernzerhof [30] type generalized gradient approximation in the exchange–correlation functional. The cutoff energy for plane wave basis was 350 eV. The Brillouin zone was sampled by a 14 × 14 × 1 Monkhorst–Pack mesh grid. The convergence of the cutoff energy and mesh grid had been checked in our test calculations. The atomic structures were relaxed until the Feynman–Hellman force on each atom was less than 0.01 eV Å<sup>-1</sup>.

## 3. Results and discussion

CoSe grew on the TiO<sub>2</sub>-terminated SrTiO<sub>3</sub>(001) via a typical layer-by-layer mode. Figure 1(b) gives an STM topographic image taken after deposition of 1.1 UC CoSe film, showing uniform atomically flat 1 UC films with some patches of the second UC. The step height is 5.5 Å, similar to that of tetragonal phase FeSe films on SrTiO<sub>3</sub> [12]. The atomic resolution images for 1 and 2 UC CoSe films shown in figures 1(c)–(e) reveal well-defined tetragonal lattices, where each bright spot corresponds to a topmost Se atom. The corresponding fast Fourier transform (FFT) images (insets in figures 1(d) and (e), respectively) give an in-plane lattice

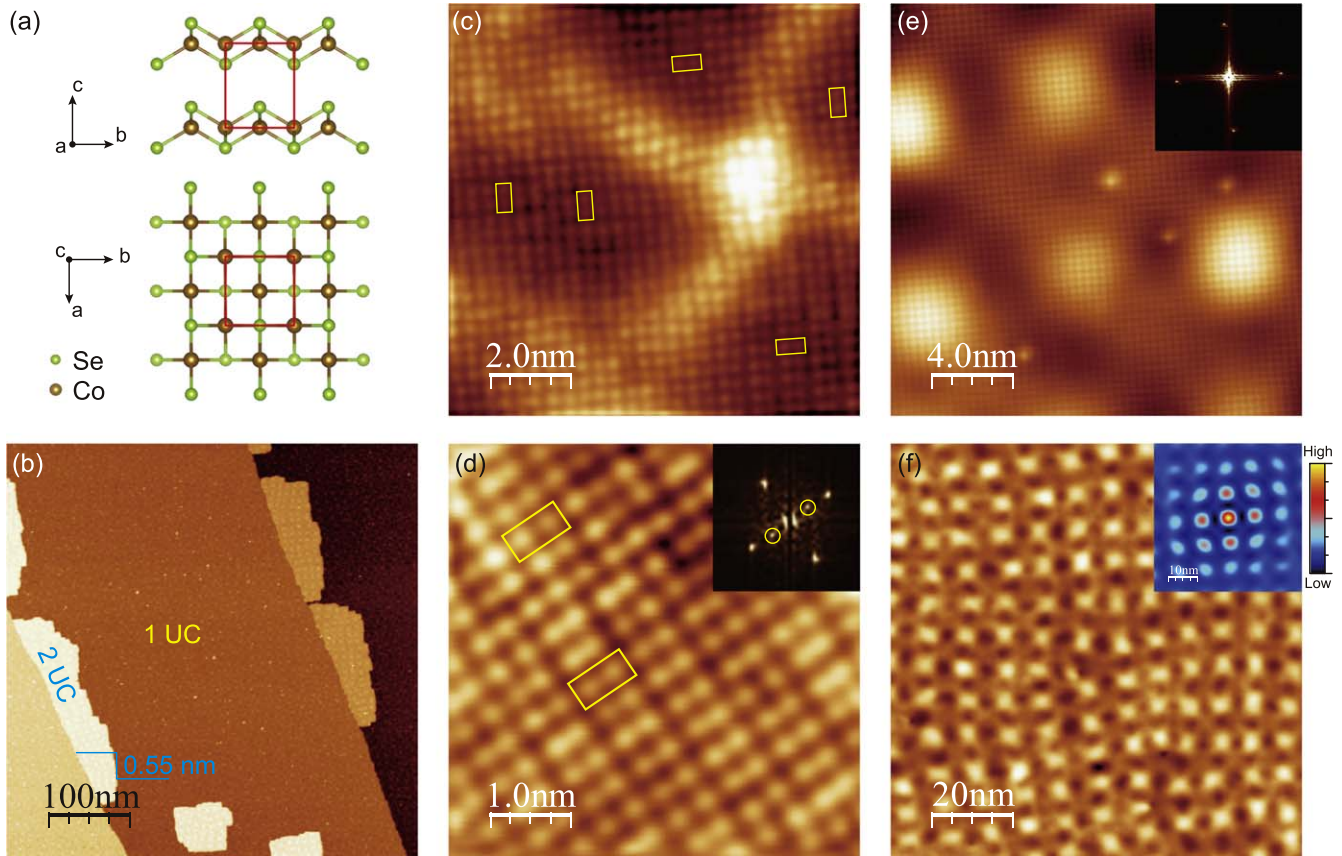


**Figure 1.** (a) Schematic structure of anti-PbO-type CoSe. The red frames indicate the unit cell. (b) STM topographic image of 1.1 UC CoSe films ( $V_s = 3$  V,  $I = 50$  pA). (c) and (d) Atomically resolved images of 1 UC CoSe films with the supercell of the  $2 \times 1$  modulation marked by yellow rectangles ((c)  $V_s = 20$  mV,  $I = 200$  pA; (d)  $V_s = -30$  mV,  $I = 200$  pA). (e) Atomically resolved image of 2 UC CoSe films ( $V_s = -50$  mV,  $I = 200$  pA). The insets in (d) and (e) are the corresponding FFT images, and the spots marked by yellow circles in (d) correspond to the  $2 \times 1$  supercell. (f) STM topographic image of 2 UC CoSe films showing Moiré patterns with self-correlation image inserted ( $V_s = 0.5$  V,  $I = 100$  pA).

constant of  $3.7 \pm 0.1$  Å, similar to that of tetragonal FeSe [12] again and smaller than the value of 3.9 Å for SrTiO<sub>3</sub>(001). The above results demonstrate that tetragonal CoSe films with (001) orientation, consisting of Se–Co–Se triple layers stacking along out-of-plane direction as schematically shown in figure 1(a), formed on SrTiO<sub>3</sub>(001). A  $2 \times 1$  modulation with respect to the Se lattice was observed on 1 UC but not on multilayer CoSe films. As demonstrated in figure 1(c), the  $2 \times 1$  modulations had two orthogonal orientations, between which formed domain boundaries that underwent strong atomic dislocation and appeared as bright stripes. Coincidentally, the same  $2 \times 1$  modulation was also observed in monolayer FeSe on SrTiO<sub>3</sub> [12] and identified as an electronic feature instead of lattice reconstruction [31].

The SrTiO<sub>3</sub>(001) surface with square lattice acts as a template and stabilizes such a tetragonal phase CoSe in the form of ultrathin films. With thickness increased to 7 UC, the step-flow layer-by-layer growth was partially replaced by spiral stacking, and hexagonal lattices formed simultaneously (figure S1(a)), indicative of a phase transition to NiAs-type structure. In this work, we focused on thin films of tetragonal CoSe. On all of them, Moiré patterns showed up due to the in-plane lattice mismatch between CoSe and SrTiO<sub>3</sub>, 3.7 Å [32] versus 3.9 Å, which became regular and ordered with increasing thickness

(figures 1(f) and S2(b), (c)). A closer examination revealed that the Moiré patterns had the same direction as the  $1 \times 1$  atomic lattices, as exemplified by the case of 2 UC shown in figure 1(f), indicating that the Moiré patterns formed basically due to lattice constant contrast instead of lattice rotation. To finely identify the in-plane lattice constant of CoSe films, we carried out a self-correlation analysis (insets of figures 1(f) and S2(b), (c), which gave the Moiré pattern periods  $L_M$  of 8.9 nm, 9.3 nm and 9.2 nm, respectively). Given that the Moiré patterns obey a relation  $N \cdot a_{\text{SrTiO}_3} = (N + 1) \cdot a_{\text{CoSe}} = L_M$ , where  $a_{\text{SrTiO}_3} = 3.905$  Å and  $N$  is an integer, we got a nice solution with  $L_M = 9.0$  nm,  $N = 23$  and  $a_{\text{CoSe}} = 3.74$  Å.

The anti-PbO-type CoSe films were intrinsically metallic, and interface charge transfer from SrTiO<sub>3</sub>(001) substrate was quite weak. As depicted in figure 2(a), the differential conductance  $dI/dV$  spectra of 1, 2 and 3 UC CoSe films consistently show dip features with finite density of states around Fermi level ( $E_F$ ), suggesting metallic nature. The spectra exhibit clear intensity peaks at around 0.2,  $-0.02$ ,  $-0.8$  eV and broad ones roughly centered at  $-0.5$  eV, which exhibited different variation with thickness. The pronounced peaks at around 0.2 and  $-0.02$  eV shifted little in energy with thickness, whereas the broad peak around  $-0.5$  eV shifted weakly



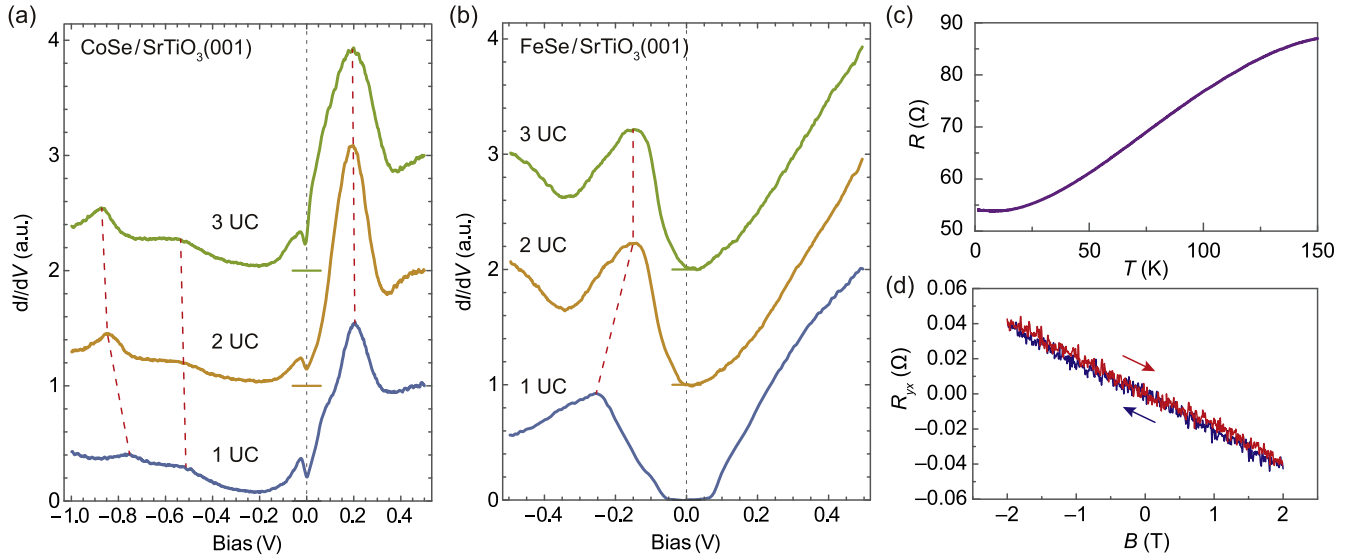


**Figure 2.** (a) The typical differential tunneling spectra of 1, 2 and 3 UC CoSe films on SrTiO<sub>3</sub>(001) taken at 4.8 K ( $V_s = 0.5$  V,  $I = 1$  nA). (b) The typical differential tunneling spectra of 1, 2 and 3 UC FeSe films on SrTiO<sub>3</sub>(001) taken at 4.8 K ( $V_s = 0.5$  V,  $I = 50$  pA). In (a) and (b), the horizontal bars indicate the zero-conductance of each curve with the same color. (c) Temperature dependence of the resistance and (d) Hall resistance as a function of external magnetic field measured at 1.6 K for 5 UC CoSe films.

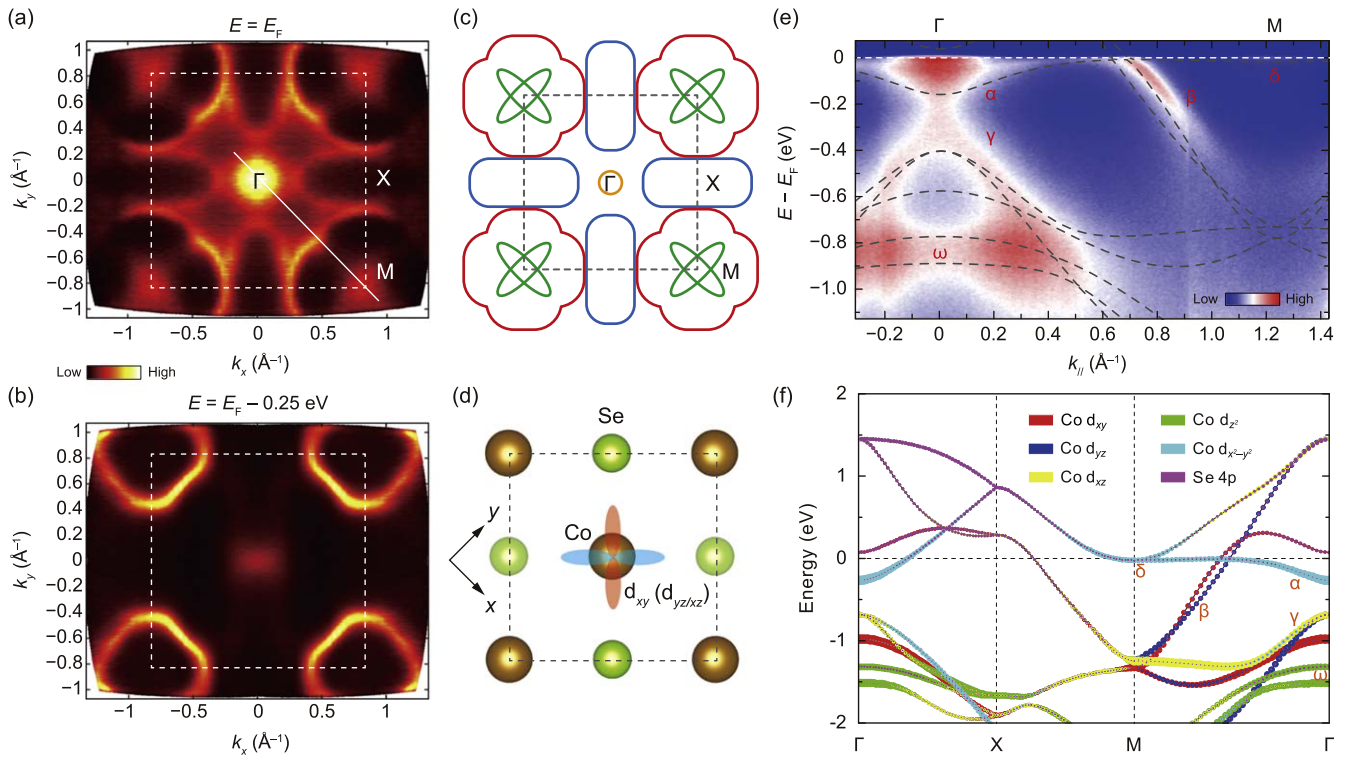


**Figure 3.** (a) and (b) The ARPES intensity maps of 1 UC CoSe at  $E_F$  and  $E_F - 0.25$  eV, respectively, measured at 100 K. (c) Schematic of the Fermi surface topology. (d) Schematic configuration of the 2-Co unit cell of CoSe with  $d_{xy}$ -type orbitals coupled strongly with the Se atoms, where the axes are chosen along the Co-Co directions. (e) Intensity plot of band dispersions along the  $\Gamma$ -M direction shown as the solid line in (a), measured at 5 K. The gray dashed lines are calculated bands for the paramagnetic phase renormalized with a factor of 1.7. (f) DFT calculated band structures of monolayer CoSe in paramagnetic phase. The contributions of the  $d_{z^2}$ ,  $d_{x^2-y^2}$ ,  $d_{xy}$ ,  $d_{yz}$  and  $d_{xz}$  orbitals of Co and 4p orbitals of Se are highlighted with different colors. The contribution weight is represented by the size of the dots.

and the peak around  $-0.8$  eV moved remarkably towards the  $E_F$  with decreasing thickness, especially between 2 and 1 UC (shifted by  $\sim 0.1$  eV). For comparison, the spectra of 1–3 UC FeSe films on SrTiO<sub>3</sub> are shown in figure 2(b). The spectral

peak in occupied state of 1 UC FeSe films was at  $-0.25$  eV, which was 0.1 eV further away from  $E_F$  compared with multilayer films, as a result of an exclusive electron transfer of  $0.12 e^-$  per Fe atom in 1 UC FeSe films from SrTiO<sub>3</sub>

substrates [14]. In contrast, the reverse relative shift in occupied states of 1 and 2 UC CoSe films could indicate a shrink of bandwidth rather than interface electron transfer. This is reasonable since the Co 3d<sup>7</sup> configuration has one more electron compared with Fe 3d<sup>6</sup>. Consequently, the intrinsic electron filling shifts up chemical potential. This scenario is confirmed by ARPES results and first-principles calculations, as discussed below.

The ARPES measurements revealed band structures of monolayer CoSe films on SrTiO<sub>3</sub>(001). Figures 3(a) and (b) show the ARPES intensity maps at  $E_F$  and  $E_F - 0.25$  eV, respectively, and figure 3(e) the band dispersions along the M– $\Gamma$ –M direction measured at 5 K. As shown in figure 3(e), the band structure consists of hole bands  $\gamma$  and  $\omega$  at the  $\Gamma$  point below the Fermi level, electron bands  $\alpha$  at the  $\Gamma$  point and  $\beta$  at the M point crossing the Fermi level. This band structure bears extraordinary resemblance to that of 1 UC FeSe on SrTiO<sub>3</sub> [8, 33], except that the Fermi level shifts upward by  $\sim 0.25$  eV as a result of one more electron filling in the 3d shell. The similarity is further seen from the constant energy map at  $E_F - 0.25$  eV (figure 3(b)), which shows large electron pockets at M points and minimized spectral weight at  $\Gamma$  point, in good agreement with the Fermi surface of K<sub>x</sub>Fe<sub>2–y</sub>Se<sub>2</sub> [34, 35] and 1 UC FeSe on SrTiO<sub>3</sub> [8]. Combining the band dispersions in figure 3(e), we recognized the Fermi surface topology for monolayer CoSe on SrTiO<sub>3</sub>(001) from ARPES intensity map shown in figure 3(a) and sketched it in figure 3(c). It consists of one circular electron pocket around the  $\Gamma$  point, one large electron pocket surrounding two fusiform electron pockets around the M point, and one elliptical hole pocket around X point.

Our DFT calculations, in combination with ARPES results, demonstrate very weak interface charge transfer and weakened electronic correlation in monolayer CoSe compared with electron-doped FeSe. We first performed DFT calculations for monolayer CoSe on SrTiO<sub>3</sub>(001). The corresponding Bader analysis shows that the charge transferred from SrTiO<sub>3</sub> to monolayer CoSe is only 0.026 electrons per Co atom, in stark contrast to 0.12 electrons per Fe atom in monolayer FeSe [14]. We then simplified the calculations to free-standing monolayer CoSe with the in-plane lattice constant of 3.75 Å as resolved from STM topographic images. We calculated both paramagnetic and ferromagnetic phases and found that paramagnetic phase had a slightly higher (18 meV per Co atom) total energy. However, the calculated band structures in a ferromagnetic state show spin splitting of  $\sim 0.3$  eV (figure S3), which was not observed by APRES. In contrast, the calculations of paramagnetic state reproduce the ARPES features well. Figure 3(f) depicts the band structures and their orbital configuration of monolayer CoSe in paramagnetic state, where the Brillouin zone is regarded to a two-Co unit cell as displayed in figure 3(d). The calculated band structures with a renormalization factor of 1.7 are overlaid in figure 3(e) as dashed lines. In figure 3(f), the different colors highlight the contributions from Co 3d and Se 4p orbitals. Clearly, all the 3d orbitals of Co contribute to the bands near

the Fermi level. The  $\alpha$  ( $\delta$ ) and  $\omega$  bands are dominated by  $d_{x^2-y^2}$  and  $d_{z^2}$  orbitals, respectively. The  $\beta$  and  $\gamma$  bands are composited by the  $t_{2g}$  bands ( $d_{xy}$ ,  $d_{yz}$  and  $d_{zx}$ ), which are strongly bonded with the 4p orbitals of the Se atoms at the corners of CoSe<sub>4</sub> tetrahedral (figure 3(d)). The renormalization factor 1.7 is smaller than 2.5 for K<sub>x</sub>Fe<sub>2–y</sub>Se<sub>2</sub> [34], suggestive of weaker electronic correlation in the former. This is further revealed from the comparison of bandwidth: the bandwidth of the hole band  $\gamma$  at  $\Gamma$  point for monolayer CoSe films is 0.5 eV (figure 3(e)), much larger than the values of 0.15 eV for monolayer FeSe/SrTiO<sub>3</sub> [36] and 0.14 eV for K<sub>0.77</sub>Fe<sub>1.65</sub>Se<sub>2</sub> [37].

It is worth emphasizing that the tetragonal CoSe films were probably paramagnetic, contrasting with the bulk counterpart that undergoes ferromagnetic transition at 10 K [32]. Besides the agreement of band structures revealed by ARPES with DFT calculations, the nonmagnetic phase of tetragonal CoSe films is further supported by transport results. Displayed in figures 2(c) and (d) are the temperature dependence of resistance and Hall resistance at 1.6 K as a function of magnetic field for 5 UC CoSe films. The resistance behavior demonstrates normal metal feature, while the Hall resistance shows a linear dependence on magnetic field without magnetic hysteresis at all. This suggests that the original ferromagnetism in 3D material was suppressed with evolution to 2D films, probably resulting from in-plane Co–Co distance variation due to substrate strain effect or interlayer coupling modulation in 2D form. In addition, the Hall coefficient was negative, indicating electron dominated charge carriers, consistent with our ARPES results.

At last, we address the analog of monolayer CoSe films to high temperature superconductors, in particular to monolayer FeSe superconductor, and discuss the possibility of achieving superconductivity therein. First, there is an empirical principle for cuprates and iron-based superconductors [38]: the quasi-two dimensional electronic environment must be dominated by the d orbitals with the strongest in-plane d–p hybridization near  $E_F$ . Specifically, for anti-PbO-type FeSe and CoSe where 3d metal atoms sit in the Se tetrahedrals, the  $d_{xy}$ -type orbitals that form the large electron bands  $\beta$  at M points are vital to their superconductivity. All the electron-doped FeSe materials that undergo superconducting transitions above 30 K [6, 8, 39–41] share a common band feature: the Fermi level lies between the  $\alpha$  and  $\gamma$  bands, leaving the  $\beta$  band half-filled and isolated at  $E_F$ . Similarly, monolayer CoSe on SrTiO<sub>3</sub> could fit such condition after a rigid band upshift of  $\sim 0.25$  eV. Second, the monolayer CoSe does not show ferromagnetism at low temperature, which is beneficial to the emergence of superconductivity. Third, as a result of the Co 3d<sup>7</sup> configuration, with the  $t_{2g}$  orbitals tuned away from half filling, monolayer CoSe films exhibit high carrier density and weak electronic correlation compared with FeSe/SrTiO<sub>3</sub>. The concomitance between high carrier density and weak electronic correlation follows the normal trend in the over-doped regime for most cuprates and iron-based superconductors [37], i.e. becoming more Fermi-liquid like as the correlation strength decreases.

Thus, with inverse doping, the electron properties might be recovered to an optimal level. Based on the above features, we deduce that the 2D CoSe thin films may host superconductivity upon hole doping. It is worth noting that the SrTiO<sub>3</sub> substrate here acts as a template to stabilize the tetragonal CoSe thin films, but does not induce strong charge transfer to CoSe films. The results we observed here mainly show the intrinsic properties of tetragonal CoSe films. Through interfacing with some oxides that have tetragonal structures and can act as hole reservoirs, just like the case in hole-doped cuprates, the CoSe layer could probably become superconducting. Besides such interface engineering, ion liquid gating and chemical substitutions (e.g., Mn substitution of Co or As substitution of Se), are also promising routes to realizing superconductivity in CoSe films. Moreover, replacing Fe with Co will lead to changes in Hund's coupling, onsite Hubbard potential and crystal electric field. Direct contrastive study on tetragonal phase CoSe and FeSe provides a chance to find the dominant factors more than electronic features in the high  $T_c$  superconductivity.

#### 4. Conclusion

In summary, by using MBE and choosing SrTiO<sub>3</sub>(001) as substrate, we obtained layered CoSe ultrathin films with anti-PbO-type structure, identical to the basic building blocks of high  $T_c$  iron-based superconductors. STS and ARPES results of CoSe films showed similar band structures to the high temperature interface superconductor, monolayer FeSe films on SrTiO<sub>3</sub>, except for an 0.25 eV shift-up of the Fermi level and enlarged bandwidth. We propose that superconductivity might be realized in CoSe thin films with hole doping via well controlled chemical substitution, ion liquid gating or interface engineering. The tetragonal CoSe film, as a new 2D material realized due to interface effect, could probably implement a family with iron-based and nickel-based superconductors, and the contrastive studies may carve out a way to explore the mechanism of unconventional superconductors.

#### Acknowledgments

This work was supported by the National Natural Science Foundation of China (11574174, 11774193, 11790311, and 11474030), and the National Basic Research Program of China (2015CB921000).

#### ORCID iDs

Chong Liu  <https://orcid.org/0000-0002-2314-8687>

Wei Li  <https://orcid.org/0000-0003-4409-7185>

Lili Wang  <https://orcid.org/0000-0001-6035-1660>

#### References

- [1] Chu C W, Deng L Z and Lv B 2015 *Physica C* **514** 290–313
- [2] Paglione J and Greene R L 2010 *Nat. Phys.* **6** 645–58
- [3] Zhang H and Sato H 1993 *Phys. Rev. Lett.* **70** 1697–9
- [4] Takahashi H, Igawa K, Arii K, Kamihara Y, Hirano M and Hosono H 2008 *Nature* **453** 376–8
- [5] Hsu F C *et al* 2008 *Proc. Natl Acad. Sci. USA* **105** 14262–4
- [6] Guo J, Jin S, Wang G, Wang S, Zhu K, Zhou T, He M and Chen X 2010 *Phys. Rev. B* **82** 180520
- [7] Lu X F *et al* 2015 *Nat. Mater.* **14** 325–9
- [8] He S *et al* 2013 *Nat. Mater.* **12** 605–10
- [9] Reyren N *et al* 2007 *Science* **317** 1196–9
- [10] Locquet J P, Perret J, Fompeyrine J, Machler E, Seo J W and Van Tendeloo G 1998 *Nature* **394** 453–6
- [11] Gozar A, Logvenov G, Kourkoutis L F, Bollinger A T, Giannuzzi L A, Muller D A and Bozovic I 2008 *Nature* **455** 782–5
- [12] Wang Q-Y *et al* 2012 *Chin. Phys. Lett.* **29** 037402
- [13] Huang D and Hoffman J E 2017 *Annu. Rev. Condens. Matter Phys.* **8** 311–36
- [14] Tan S *et al* 2013 *Nat. Mater.* **12** 634–40
- [15] Lee J-J *et al* 2014 *Nature* **515** 245–8
- [16] Naritsuka M *et al* 2018 *Phys. Rev. Lett.* **120** 187002
- [17] Tang C *et al* 2016 *Phys. Rev. B* **93** 020507
- [18] Kordyuk A A, Zabolotnyy V B, Evtushinsky D V, Yaresko A N, Büchner B and Borisenko S V 2013 *J. Supercond. Novel Magn.* **26** 2837–41
- [19] Damascelli A, Hussain Z and Shen Z-X 2003 *Rev. Mod. Phys.* **75** 473–541
- [20] Ronning F, Kurita N, Bauer E D, Scott B L, Park T, Klimczuk T, Movshovich R and Thompson J D 2008 *J. Phys.: Condens. Matter* **20** 342203
- [21] Wang H, Dong C, Mao Q, Khan R, Zhou X, Li C, Chen B, Yang J, Su Q and Fang M 2013 *Phys. Rev. Lett.* **111** 207001
- [22] Sakurai H, Ihara Y and Takada K 2015 *Physica C* **514** 378–87
- [23] Mizoguchi H, Kuroda T, Kamiya T and Hosono H 2011 *Phys. Rev. Lett.* **106** 237001
- [24] Yang J, Chen B, Wang H, Mao Q, Imai M, Yoshimura K and Fang M 2013 *Phys. Rev. B* **88** 064406
- [25] Bøhm F, Grønvald F, Haraldsen H and Prydz H 1955 *Acta Chem. Scand.* **9** 1510–22
- [26] Blöchl P E 1994 *Phys. Rev. B* **50** 17953–79
- [27] Kresse G and Joubert D 1999 *Phys. Rev. B* **59** 1758–75
- [28] Blöchl P E, Först C J and Schimpl J 2003 *Bull. Mater. Sci.* **26** 33–41
- [29] Kresse G and Furthmüller J 1996 *Phys. Rev. B* **54** 11169–86
- [30] Perdew J P, Burke K and Ernzerhof M 1996 *Phys. Rev. Lett.* **77** 3865–8
- [31] Li N, Li Z, Ding H, Ji S, Chen X and Xue Q-K 2013 *Appl. Phys. Express* **6** 113101
- [32] Zhou X, Wilfong B, Vivanco H, Paglione J, Brown C M and Rodriguez E E 2016 *J. Am. Chem. Soc.* **138** 16432–42
- [33] Liu D *et al* 2012 *Nat. Commun.* **3** 931
- [34] Qian T *et al* 2011 *Phys. Rev. Lett.* **106** 187001
- [35] Zhang Y *et al* 2011 *Nat. Mater.* **10** 273
- [36] Liu X *et al* 2014 *Nat. Commun.* **5** 5047
- [37] Ye Z R *et al* 2014 *Phys. Rev. X* **4** 031041
- [38] Hu J 2016 *Sci. Bull.* **61** 561–9
- [39] Miyata Y, Nakayama K, Sugawara K, Sato T and Takahashi T 2015 *Nat. Mater.* **14** 775–9
- [40] Wen C H *et al* 2016 *Nat. Commun.* **7** 10840
- [41] Zhao L *et al* 2016 *Nat. Commun.* **7** 10608